JOURNAL OF CHEMICAL INFORMATION AND MODELING

Article

pubs.acs.org/jcim

Computational Study of Drug Binding Affinity to Influenza A Neuraminidase Using Smooth Reaction Path Generation (SRPG) Method

Hung Nguyen,[†] Tien Tran,[‡] Yoshifumi Fukunishi,[§] Junichi Higo,[∥] Haruki Nakamura,[∥] and Ly Le*[,†,⊥]

[†]Life Science Laboratory, Institute for Computational Science and Technology, Ho Chi Minh City, Vietnam

[‡]University of Technology, Ho Chi Minh City, Vietnam

[§]National Institute of Advanced Industrial Science and Technology, Tokyo, Japan

[∥]Institute for Protein Research, Osaka University, Osaka, Japan

[⊥]School of Biotechnology, International University, Vietnam National University, Ho Chi Minh City, Vietnam

Supporting Information

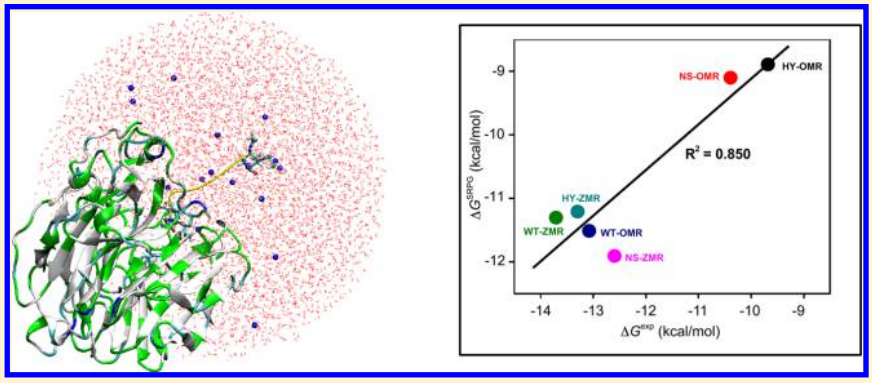

ABSTRACT: Assessment of accurate drug binding affinity to a protein remains a challenge for *in silico* drug development. In this research, we used the smooth reaction path generation (SRPG) method to calculate binding free energies and determine potential of mean forces (PMFs) along the smoothed dissociation paths of influenza A neuraminidase and its variants with oseltamivir (Tamiflu) and zanamivir (Relenza) inhibitors. With the gained results, we found that the binding free energies of neuraminidase A/H5N1 in WT and two mutants (including H274Y and N294S) with oseltamivir and zanamivir show good agreement with experimental results. Additionally, the thermodynamic origin of the drug resistance of the mutants was also discussed from the PMF profiles.

1. INTRODUCTION

The avian influenza (H5N1) has the likelihood of causing a human influenza pandemic, which has impacted the worldwide society and economy.[1−3] Hence, finding a possible treatment and prevention against influenza H5N1 is becoming the major consideration of many studies. Neuraminidase (NA) (also known as sialidase), a viral enzyme that plays a key role in the life cycle of influenza viruses, would be the main stream of pharmacological strategies in the process of treating influenza. At present, three FDA-approved drugs (oseltamivir, zanamivir, and peramivir) to treat influenza A/H5N1 have been discovered and developed based on the structural information on neuraminidase.[4,5] After several years of clinical experience, the drugs have worked effectively on the wild type neuraminidase of avian influenza H5N1. However, oseltamivir resistance on two mutations, H274Y and N294S, of the flu virus have been reported. Here, the H274Y and N294S mutants were found to induce strong and mild drug resistance, respectively, to oseltamivir, but neither of them alter significantly the binding affinity for another antiviral drug, zanamivir.[5]

Even though several studies on drug binding affinity and the pathway to neuraminidases have been done, the problem of drug resistance is still not fully understood. For binding affinity, a group from Chulalonkon University has performed a 10 ns molecular dynamic simulation and molecular mechanics/Poisson−Boltzmann surface area (MM-PBSA) calculations for those ligands to wild type and H274Y neuraminidases. The findings were that the hydrophobic interaction of the bulky pentyl group is suggested to be the main source of oseltamivir resistance in the H274Y mutant.[6] Another research on oseltamivir−neuraminidase complexes also used molecular dynamics (MD) with a Hamiltonian replica exchange to calculate the change in binding free energy for H274Y, N294S, and Y252H mutants. Contrary to previous studies, they suggested that drug resistance

Received: May 27, 2015
Published: August 6, 2015

DOI: 10.1021/acs.jcim.5b00319
J. Chem. Inf. Model. 2015, 55, 1936−1943

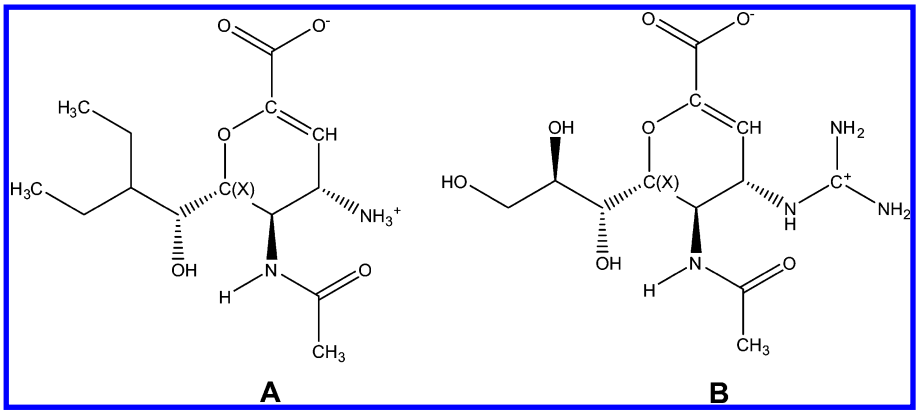

Figure 1. Oseltamivir (OMR) (A) and zanamivir (ZMR) (B) structures. The carbon atoms C(**X**) were selected as "landmark atom".

mutations in NA led to subtle rearrangements in the protein structure and its dynamics that together alter the active-site electrostatic environment and modulate inhibitor binding.[7−12] Regarding the drug binding pathway, there are conflicts in the study by the group at UCSD[13] and Le et al.[14] While Sung et al. using Brownian dynamics suggested a pathway through the 430-loop cavity, Le et al. suggested other negatively charged pathways using steered molecular dynamics (SMD) and the average electrostatic potential. More accurate binding affinities of drug candidates are needed for rational drug design against H5N1 variants.

The free energy profile expressed along an appropriate reaction coordinate is called the potential of mean force (PMF), which could provide a useful insight for understanding the protein−ligand binding mechanism and affinity. Therefore, many different methods were developed to calculate PMFs for protein−ligand binding, such as the filling potential (FP) method,[15] metadynamics method,[16,17] MP-CAFEE method,[18] Jarzynski's method,[19] and smooth reaction path generation (SRPG) method.[20]

In this study, the SRPG method was employed to determine the binding free energy between oseltamivir and zanamivir drugs and three A/H5N1 neuraminidases (including wild type, WT, and two oseltamivir-resistant mutants, H274Y and N294S). The SRPG method will generate a protein−ligand binding pathway by taking off each ligand from the bound position to far outside of protein using the FP method[15] and approximates it by a smooth line. Then, thermodynamic integration is conducted along the smooth path to determine the PMF with additional entropic correction terms, providing the binding free energy for each protein−ligand complex. The gained results will be compared with the experimental results.

2. MATERIALS AND METHODS

2.1. Materials. The 3D structures of six complexes were constructed from H5N1 neuraminidase, including wild type (WT) and two mutant variants (H274Y (HY) and N294S (NS) mutants) with two drugs (including oseltamivir (OMR) (Figure 1A) and zanamivir (ZMR) (Figure 1B). These structures were taken from Protein Data Bank (PDB) with PDB entry codes: 2HU4 (WT-OMR), 3CL0 (HY-OMR), 3CL2 (NS-OMR), and 3CKZ (HY-ZMR).[5,21] Two complex structures of the wild type and N294S mutant with ZMR (WT-ZMR and NS-ZMR) were constructed as follows: We extracted ZMR from the 3CKZ complex and optimized it with the Gaussian 98 software[22] to determine atomic charges of the ligands. The details are described in the Computational Method section. Then, ZMR was docked to the active sites of the WT and N294S mutant by Autodock 4.0,[23] taking receptors from 2HU4 and 3CL2 complexes, respectively. The docking process is described as follows:

Preparing the Structures. Visual molecular dynamics (VMD)[24] was used to visualize and separate the receptor from 2HU4 and 3CL2 complexes for docking. Autodock tools (ADT) were used to convert the receptors and ZMR in the PDB format to the pdbqt format with the correction of charges for docking.

Docking Process. The docking procedure requires the identification of the binding box position—the active site of the proteins. This was done by using the crystal structure of the protein with bound ZMR. The grid box for protein−ligand docking was designed to fit the protein surface.

Choosing the Structures. The docking results were analyzed and ranked by lowest binding energy. Additionally, we also calculated RMSD values between the heavy-atom coordinates of the docked ligand and the ligand in X-ray structure. The RMSD values corresponded to 0.073 and 0.012 Å for WT-ZMR and NS-ZMR, respectively. These values showed that the ligand docking calculations were successfully done (a RMSD value less than 2 Å is thought to be successful).[25−27] Thus, the generated structures by Autodock 4.0 were used in the current study.

2.2. Computational Method. We employed the SRPG method to calculate PMFs and binding energies of the six complexes by performing MD simulations at 300 K.

Smooth Reaction Path Generation (SRPG) Method. For each simulated complex model, the SRPG method calculates binding free energy through three steps:[20] (Step 1) Generate a smooth dissociation path of a ligand from the protein binding site. Smoothness makes the numerical error small. (Step 2) Estimate the mean force acting on a landmark atom defined in the ligand at each position of the smooth path with performing dissociation simulation along the path. (Step 3) Calculate the free energy surface around the bound state.[15]

The binding free energy is calculated by integrating the mean force along the path. This free energy is corrected by the binding free energy obtained from Step 3 and a free energy for the free-state ligand, which moves a large volume in solution without feeling a force from the protein. Then, the resultant free energy value is comparable with an experimental free-energy difference for dissociation.

Step 1: Generating Rough Compound Dissociation Path. The ligand dissociation path links the bound and unbound states of ligand. To obtain the ligand dissociation path, a rough MD simulation is performed with a starting conformation of the protein−ligand complex at 300 K *in vacuo* with a short cutoff of 1−5 van der Waals and Coulomb interactions. The filling

DOI: 10.1021/acs.jcim.5b00319
J. Chem. Inf. Model. 2015, 55, 1936−1943

potential method (FP)[15] is used to enable the ligand to drift from the bound position to the unbound position automatically. Here, a rough dissociation path is obtained. One of the ligand atoms is selected as a landmark atom to represent the ligand position. The landmark atom is a heavy atom near the center of mass of the ligand, and the coordinates of the n-th position of the rough dissociation path is denoted as $\mathbf{p}^0(n)$. The dissociation path is described by $\{\mathbf{p}^0(n); n = (1, 2, 3,..., M)\}$, where M is the number of trajectory frames.[20] In Figure 1, the landmark atoms in OMR and ZMR are shown by the carbon atom **X**.

Step 2: Constructing a Smooth Dissociation Path and PMF along the Path. Once a dissociation path is defined, a thermodynamic integration (TI) technique[15] is applicable to calculate the binding free energy. In principle, this path could be arbitrary selected because the free energy is a thermodynamic quantity, i.e., the free energy difference between the initial and final states is independent to the path. Practically, however, a ragged pathway may introduce numerical errors in the resultant free energy. Thus, a smooth reaction path instead of the rough dissociation path $\{\mathbf{p}^0(n); n = (1, 2, 3,..., M)\}$ is needed to accurately perform the TI method. Then, the rough dissociation path obtained previously is smoothed by Legendre polynomials, which round the roughness of the path. With one-parameter reaction path is described as $\mathbf{p}(t) = \{p_x(t), p_y(t), p_z(t); t = [0, 1]\}$. In detail, that is defined by

$$p_x(t) = \sum_{L}^{i=0} c_x^i p_i(t)$$
$$p_y(t) = \sum_{L}^{i=0} c_y^i p_i(t)$$
$$p_z(t) = \sum_{L}^{i=0} c_z^i p_i(t) \quad (1)$$

where $p_i(t)$ is i-th Legendre function with $0 \le t \le 1$. The L value controls the curvature of the reaction path, and the path will be linear when $L = 1$. At the initial coordinate, $\mathbf{p}(0)$ and the final coordinate $\mathbf{p}(1)$ values are fixed to the original bound and unbound coordinates.

Furthermore, the Monte Carlo method is used to examine multiple paths around the rough dissociation path, which links the bound state and the unbound state. A set of discrete points on path is necessary to form intermediate states of the dissociation. N points (N states) on a smooth path are generated along the initial rough path $\mathbf{p}(t)$. If D is the distance between two points on the path, then the S value that represents the similarity to the original path is defined by

$$S = \sum_m^M \sum_n^N D(\vec{p}(n'N), \vec{p}^0(m))^2$$

Here, the S value is calculated for various values of the coefficients c_x^i, c_y^i, and c_z^i) and which has been minimized by the optimal parameter set $\{c_x^i, c_y^i, c_z^i, I = 1, 2, ..., L\}$.

The nearest path to the rough dissociation path is selected for the PMF calculation below. Now, we have the smooth path, along which the ligand dissociates, and PMF is calculated at each position of the smooth path. In addition to the initial bound state and the final unbound state, we generated 49 intermediate states along the dissociation path, and the distance between landmark atoms of two neighboring system was about 0.4 Å.

Step 3: Calculating Binding Free Energy. After computing the PMF profile along the smooth dissociation path, we calculated the binding free energy ΔG by the following equation:

$$\Delta G = G(r_0) - G(r_\infty) - k_B T \ln \frac{\frac{\sqrt{\pi}}{\sqrt{\beta k_x / 2}} \frac{\sqrt{\pi}}{\beta k_y / 2} \frac{\sqrt{\pi}}{\sqrt{\beta k_z / 2}}}{V_0} \quad (3)$$

The first term $G(r_0)$ is the PMF at $\text{rmsd}^{\text{inhibitor}} = 0$ (i.e., PMF at the complex structure), and the second $G(r_\infty)$ is the PMF at $\text{rmsd}^{\text{inhibitor}} \rightarrow \infty$ (i.e., PMF of ligand far enough from the protein). When PMF is calculated up to a position of where the slope of PMF is zero, $G(r_\infty)$ can be replaced by PMF at the zero slope. PMF values are calculated by TI method:[20]

$$G(R) = \int_0^R <\vec{F}(\vec{r})> \bullet d\vec{r} \quad (4)$$

where $\vec{F}$ and $\vec{r}$ are represented the force acting on the landmark atom and the position of the landmark atom of ligand, respectively. In detail, $F(\mathbf{r})$ is the time-averaged force acting on the compound at position $\mathbf{r}$. The compound is restrained at position $\mathbf{r}$ by an umbrella potential. Thus, $F(\mathbf{r})$ is calculated by removing the effect of the umbrella potential. The third term is a correction to take into account an entropic contribution of the ligand in the complex state. The parameters k_x, k_y, and k_z are the force constants of the energy basin at the complex state approximating the shape of the basin by a parabolic function. The V_0 is a correction term to take into account an entropic contribution of the freely moving ligand in a solution; V_0 is analytically computable and equals to1661 Å^3 at 1 M density (V_0 is a volume that one compound occupies at 1 M density. $V_0 = 1\ L/N_A$). The parameters k_B, T, β are the Boltzmann constant, temperature, and $1/k_BT$, respectively.

Molecular Dynamic Simulations. The computer program myPresto, last updated in 2014 June (version 4.304) (http://presto.protein.osaka-u.ac.jp/myPresto4/index_e.html), was used for MD simulations used in the SRPG method.[15]

All missing hydrogen atoms of the receptors and topology files were generated by the tplgene module of myPresto. Topology files of the ligands were generated by the tplgeneL module of myPresto. The atomic charges of the ligands were determined by the restricted electrostatic point charge (RESP) procedure by using Hartree−Fock (HF)/6-31 G(d) level quantum chemical theory with the Gaussian 98 program.[22] We used the parameters of the AMBER parm99 force field[28] for all receptors. Those for ligands were taken from the general AMBER force field (GAFF).[29] The system was energy-minimized with position restraint onto the backbone atoms of the protein and the landmark atom of drug. This relaxed structure was the initial position of the ligand dissociation.

Each protein−drug complex was placed in a sphere, the radius of which was 35 Å, consisting of water molecules, and the center of the water sphere was set to the center of mass of the protein−drug complex. The complexes were ionized by NaCl (0.154M) to mimic physiological condition. The TIP3P water model was adopted for water molecules.[30] In MD simulations, the SHAKE algorithm was employed to constrain all bonds between heavy and hydrogen atoms,[31] and the electrostatic interactions were computed by a fast-multipole method without truncation.[32] Canonical MD simulations were performed for these total 51 protein−drug complexes with position restraint potential onto the backbone atoms of the protein and the landmark atom of the drug. The equilibration process was performed MD simulation for 1000 ps at 300 K. The MD simulation of each system was performed with time step was 1.5 fs for 750 ps

DOI: 10.1021/acs.jcim.5b00319
J. Chem. Inf. Model. 2015, 55, 1936−1943

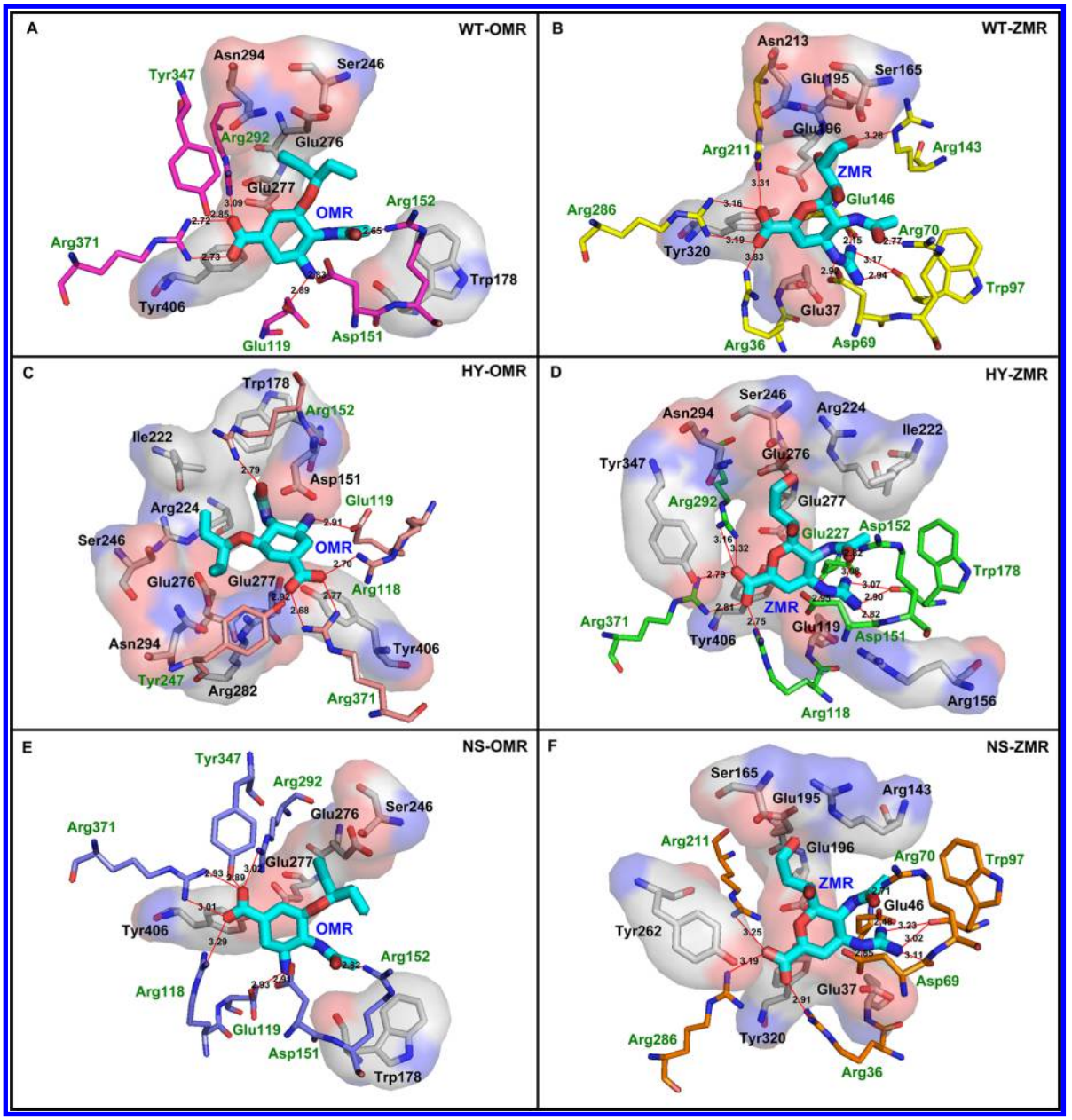

Figure 2. Drug−protein interactions for six active sites of (A) WT-OMR, (B) WT-ZMR, (C) HY-OMR, (D) HY-ZMR, (E) NS-OMR, and (F) NS-ZMR with LigPlot and PyMol software.[33−35]

of data sampling at 300 K using the leapfrog algorithm, and time-averaged forces acting on the drug of all 51 systems were calculated.

3. RESULTS AND DISCUSSION

3.1. Interactions between Active Site Residues and Drugs in WT and Mutants. All hydrogen bonds and hydrophobic interactions at the active sites in the six complexes are displayed in Figure 2A−F using LigPlot and PyMOL software.[33−35] In the WT structure, there are at least six active site residues forming an H-bond with OMR (Figure 2A) and eight active site residues forming an H-bond with ZMR (Figure 2B). In the HY mutant variant, there are five active site residues forming an H-bond with OMR (Figure 2C) and seven active site residues forming an H-bond with ZMR (Figure 2D). In the NS mutant variant, there are seven active site residues forming an H-bond with both OMR and ZMR (Figure 2E and F).

3.2. Releasing Ligands from Binding Pocket of A/H5N1 Neuraminidases. In the first step of the SRPG method, we obtained the dissociation path using the trajectories given by the filling potential (FP) method,[15] which was described by the white pipes in Figure 3. Then, we generated the smooth dissociation path starting from the bound ligand position. Here, the landmark atom of each complex system existed on the smoothest dissociation path (the yellow pipes of Figure 3 for all six complexes and Figure 4A for WT-OMR). From our prior studies using SMD[14] or slide grid box docking,[36] drug unbinding pathways were also generated. A prior study also suggested to use SMD as a tool for drug design in which the strength of pulling force applied to cause ligand dissociation is comparable with its binding affinity.[37] The advantage of the SRPG method is that it has the smoothing reaction path process, which will help to overcome limitation of discontinuity in the paths generated in docking study or bias force that

DOI: 10.1021/acs.jcim.5b00319
J. Chem. Inf. Model. 2015, 55, 1936−1943

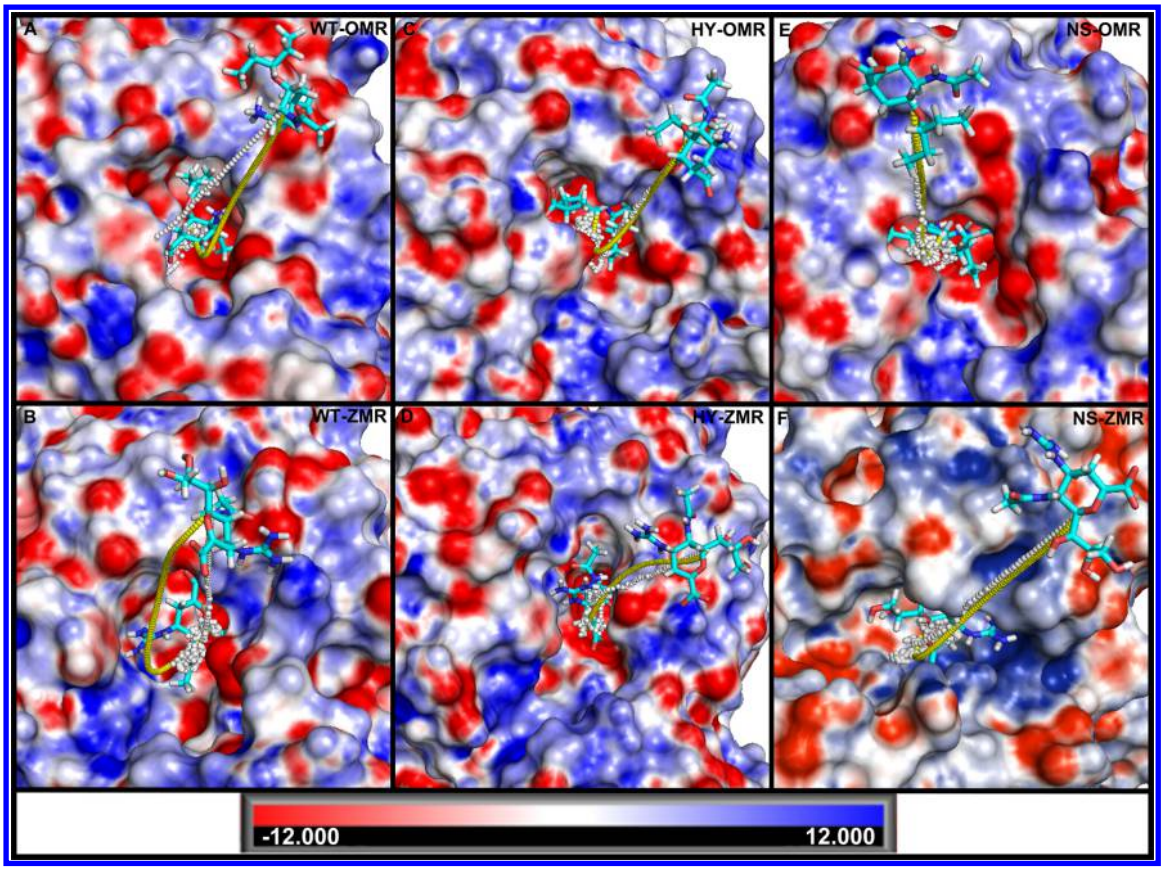

Figure 3. Smooth reaction paths determined by SRPG method for (A) WT-OMR, (B) WT-ZMR, (C) HY-OMR, (D) HY-ZMR, (E) NS-OMR, and (F) NS-ZMR. The white pipes are the linked trajectories obtained first by the FP method *in vacuo*, and the yellow pipes represent the smooth reaction paths were generated by the SRPG method.

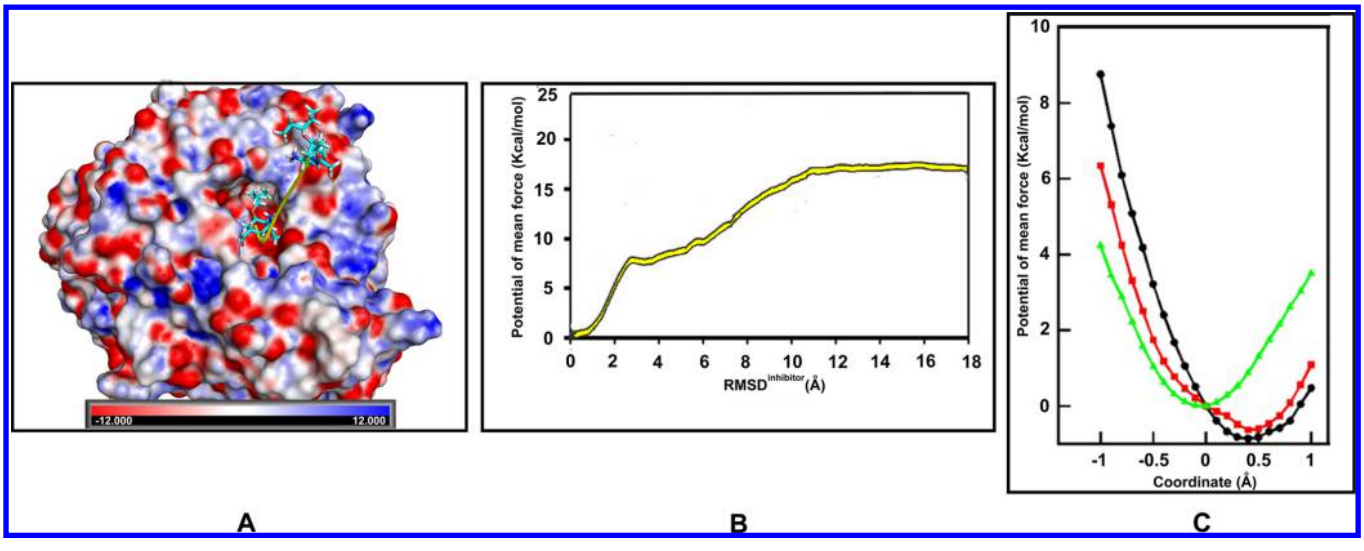

Figure 4. Procedure of the SRPG method for WT-OMR (wild type neuraminidase avian influenza H5N1 and oseltamivir (OMR). (A) Pathway of OMR moving out from the binding pocket of neuraminidase, which was moved from bound to unbound states. The yellow pipe is the resulted smooth path from the landmark atom position of the bound state to the unbound state, where $rmsd^{inhibitor}$ = 18 Å. (B) Potential of mean force (PMF) of OMR and WT neuraminidase. (C) Free energy surface around the bound state of WT-OMR complex, approximated by a three-dimensional parabola. Black line is for k_x, red line is for k_y, and green line is for k_z. The values of k_x, k_y, and k_z are 4.6, 3.8, and 3.9 (kcal/mol/Å^2), respectively (Table S1).

influenced the paths generated by SMD to produce more accurate PMF and binding energy. Accurate binding energy and detail of binding pathways of drug candidates are both critical for rational design of optimal new drugs with good binding kinetics.

In addition to the initial bound state and the final unbound state, we generated 49 intermediate state along the dissociation path. Canonical MD simulations were performed for these total 51 protein−drug systems with fixing the position of one of the atomic coordinates of the drug. Averaged forces acting on the

DOI: 10.1021/acs.jcim.5b00319
J. Chem. Inf. Model. 2015, 55, 1936−1943

Table 1. Binding Free Energies (ΔG) Obtained by SRPG Method and Experiments[16]

complexes (receptor−drug)	$G(r_0) - G(r_\infty)$ (kcal/mol)	ΔG (kcal/mol) (SRPG method)	ΔG (kcal/mol) (Experiment[20])
WT-OMR	−16.6	−11.5	−13.1
WT-ZMR	−16.6	−11.3	−13.7
HY-OMR	−14.0	−8.9	−9.7
HY-ZMR	−16.0	−11.2	−13.3
NS-OMR	−14.0	−9.1	−10.4
NS-ZMR	−16.6	−11.9	−12.6

drug of all 51 systems were calculated, and the integral of the forces gave the PMF profile along the dissociation path. These PMF profiles are shown in Figure 4B (only WT-OMR) and Figure S1 (all six complexes), where drugs were dissociated up to the positions of $\text{rmsd}^{\text{inhibitor}}$ = 18 Å along the smooth paths. Here, $\text{rmsd}^{\text{inhibitor}}$ was the RMSD value of landmark atom (**X**) of inhibitors from the native complex structures. The PMF values were flat before $\text{rmsd}^{\text{inhibitor}}$ reached 18 Å for all the systems as shown in the PMF profiles. Therefore, the simulations could cover both the bound and unbound states of the inhibitors. In other words, the upper limit of $\text{rmsd}^{\text{inhibitor}}$ = 18 Å was long enough to calculate the binding free energies. The binding free energy is proportional to the log of probability of existence. As a result, at 1 M density, unbound ligand occupies a volume in solvent. If the bound ligand occupies the same volume as the unbound ligand, the binding free energy is equal to the free energy difference between the unbound and the bound states. In reality, the coordinates of the bound ligand are very restrained in a small volume by the target protein. It means that the bound ligand loses the entropy of translation and rotation, and this entropy loss depends on the protein−ligand interaction. Thus, the last term of eq 3 represents this entropy loss caused by the protein−ligand interaction. The entropy factors at the bound state were estimated by the assumed three-dimensional parabola functions as shown in Figure 4C and Table S1. The binding free energy, ΔG, was computed following eq 3 in the Computational Method section with an additional critic entropy term. All ΔG values are shown in Table 1.

The free energy surface around the binding state was slightly anisotropic. The k_x, k_y, and k_z values ranged from 2.6 to 5.1 kcal/mol/Å^2 for all six systems, and the corresponding values of the last term in eq 3 were from 4 to 5 kcal/mol. Those differences among k_x, k_y, and k_z of each system were only 5% to 22% of ΔG, and these small differences suggest that the selection of the axes and the force constants could not give large errors to ΔG.

3.3. Binding Free Energies Estimated by SRPG Method and Experimental Values. The binding free energies of six complexes calculated by the SRPG method were quite close to the experimental results (Table 1) and have a good correlation with the correlation coefficient R^2 = 0.850 as shown in Figure S2, and the root-mean-square error (RMSE) = 1.6 kcal/mol. Therefore, the SRPG method is considered to be a promising method to correctly estimate the binding affinity between a protein and its drugs. The gained result of the OMR bound complex was more accurate than the prior calculations using MM-PBSA (RMSE = 5.0 kcal/mol),[7,38] MM-PGSA (RMSE = 4.8 kcal/mol),[7,39] SRMM (RMSE = 4.2 kcal/mol),[7] and Rosetta (RMSE = 1.7 kcal/mol).[7,40] They are slightly less accurate than SRSM/HREX (RMSE = 1.1 kcal/mol)[7,21] and SRSM (RMSE = 1.5 kcal/mol).[7]

However, the results in Table 1 also indicate that the absolute values of the calculated ΔG values were slightly underestimated in comparison with the experimental data in all six calculations. It suggests that some errors should generally exist in all of the six computations. One of the reasons for the errors may be caused by incorrect electrostatic shielding effects. In these MD simulations along the dissociation paths, solvent molecules surrounded only the protein active sites and the moving inhibitors by spheres with 35 Å radii. The larger solvent environment could provide the better PMF values. The other errors may be the assumption of the entropic contributions in the second term of the eq 3: The shape of the energy basin would be more complicated than a simple parabola, which was assumed in the current computational procedure. In other words, the ligand can take only vibrational motions in the parabola assumption. The essential parts of the SRPG method are the definition of a smooth path and the computation of the mean force along the path with the thermodynamic integration. If the electrostatic shielding and entropy of the system are revised, a better binding free energy could be obtained. In addition, the force field used in this study could lead to the errors. For example, the atomic charges could change depending on the environment, but the atomic charges were fixed to the constant values during the current simulations. The ΔG should also depend on the environmental conditions, such as pH, ionic strength, etc., which were not correctly treated in the simulations.

3.4. Thermodynamic Origin of Drug Resistance of H274Y and N294S. In this study, we quantitatively confirmed that the absolute values of binding free energies of H274Y and N294S significantly decreased for OMR from those of WT but not for ZMR. From the static natures given by the complex crystal structure of the H274Y mutant protein with OMR, it was reported that the bulkier Tyr side-chain pushes the carboxyl group of Glu276 into the binding site, where a hydrophobic pentyloxy substituent of OMR is located.[21,41] On the contrary, the polar group of ZMR could interact with the carboxyl group of Glu276, so that the ZMR position changes only slightly in the complex crystal structure of H274Y with ZMR. For the N294S mutant protein, an aromatic group of Tyr347 was reported to make a slight structural change to give putatively weaker hydrogen bond interactions with OMR due to the mutation of Asn294 with Ser residue.

Those static complex structures would explain why the complexes of WT-OMR and WT-ZMR are structurally stable but those with the drug-resistant mutant proteins, HY-OMR and NS-OMR, are less stable. However, the thermodynamic origin of the drug resistance has been still unclear. Although the binding free energy does not depend on the dissociation paths in the thermodynamic integration in principle, the analysis of the dissociation paths, in addition to the free energy surface around the bound state that were obtained by the FP method, may provide some hints for further mechanism of the drug resistance.

The PMFs along the dissociation paths for WT-OMR, HY-OMR, and NS-OMR are shown in Figure S1 of the Supporting Information. For WT-OMR, the first free energy barrier is clearly seen at 2.8 Å $\text{rmsd}^{\text{inhibitor}}$ with 7.9 kcal/mol. On the contrary, in HY-OMR and NS-OMR, the PMF increased almost monotonically

DOI: 10.1021/acs.jcim.5b00319
J. Chem. Inf. Model. 2015, 55, 1936−1943

with increasing $rmsd^{inhibitor}$. Thus, the unbinding of OMR from H274Y or N294S is relatively smoother than that in WT-OMR, suggesting less force is required for unbinding the inhibitor. In the case for unbinding of ZMR, all of the PMF profiles showed peaks at $rmsd^{inhibitor}$ of about 3 Å for WT-ZMR, HY-ZMR, and NS-ZMR. Namely, it seems that ZMR struggles to escape from the binding sites of WT and other mutant proteins. In addition, it is clear that the force acting on ZMR switched from attractive to repulsive with increasing $rmsd^{inhibitor}$. Thus, it is suggested that the unbinding procedures of ZMR are more complicated than those of OMR.

4. CONCLUSIONS

The aim of this study was using the SRPG method to generate PMFs along the dissociation paths and to predict binding free energies of influenza A neuraminidase and its variants with oseltamivir (OMR) and zanamivir (ZMR). We found that the binding free energies calculated by the SRPG method were in good agreement to the experimental results and the small average error about 1.6 (kcal/mol) between the computed and experimental values, although the absolute values of the calculated binding energies were slightly underestimated in all six complexes. The thermodynamic origins of the drug resistance on HY and NS mutants were discussed with the PMF curves along the dissociation paths. In particular, it is found that unbinding of OMR from HY or NS is relatively smoother than that in WT. Namely, less force may be required for unbinding the inhibitor. On the contrary, for unbinding of ZMR, all of the PMF profiles showed peaks at $rmsd^{inhibitor}$ of about 3 Å for WT and the two mutant variants, and it seems that ZMR struggles to escape from the binding sites of WT and the mutants.

■ ASSOCIATED CONTENT

Supporting Information

The Supporting Information is available free of charge on the ACS Publications website at DOI: 10.1021/acs.jcim.5b00319.

Additional figures including the detailed description of oseltamivir (OMR) and zanamivir (ZMR) structures, all hydrogen bonds and hydrophobic interactions at the active sites in six complexes, typical snapshots of smooth reaction paths determined by the SRPG method for six complexes, and binding free energy values obtained by the SRPG method of six complexes. The potential of mean forces (PMFs) along smooth paths for WT-OMR, WT-ZMR, HY-OMR, HY-ZMR, NS-OMR, and NS-ZMR (Figure S1), correlation between the binding free energy by the current SRPG method ΔG_{SRPG} and experimental ΔG^{exp} (Figure S2), and parameters in parabola functions for free energy surfaces around bound states (Table S1) provided. (PDF)

■ AUTHOR INFORMATION

Corresponding Author

*E-mail: ly.le@hcmiu.edu.vn.

Author Contributions

Hung Nguyen and Tien Tran contributed equally to this work.

Notes

The authors declare no competing financial interest.

■ ACKNOWLEDGMENTS

This work was supported by International Collaboration grants of Institute for Protein Research at the Osaka University and the grant for Development of core technologies for innovative drug development based upon IT, the Ministry of Economy, Trade, and Industry (METI) of Japan. It was also supported by the Department of Science and Technology at Ho Chi Minh City, Vietnam, under grant number 121/TB-SKHCN.

■ REFERENCES

(1) Tam, J. S. Influenza A (H5N1) in Hong Kong: An Overview. *Vaccine* **2002**, *20*, S77−S81.

(2) Ferguson, N. M.; Fraser, C.; Donnelly, C. A.; Ghani, A. C.; Anderson, R. M. Public Health Risk from the Avian H5N1 Influenza Epidemic. *Science* **2004**, *304*, 968−969.

(3) Yen, H. L.; Webster, R. G. Pandemic Influenza as a Current Threat. *Curr. Top Microbiol. Immunol.* **2009**, *333*, 3−24.

(4) von Itzstein, M. The War against Influenza: Discovery and Development of Sialidase Inhibitors. *Nat. Rev. Drug Discovery* **2007**, *6*, 967−974.

(5) Russell, R. J.; Haire, L. F.; Stevens, D. J.; Collins, P. J.; Lin, Y. P.; Blackburn, G. M.; Hay, A. J.; Gamblin, S. J.; Skehel, J. J. The Structure of H5N1 Avian Influenza Neuraminidase Suggests New Opportunities for Drug Design. *Nature* **2006**, *443*, 45−49.

(6) Malaisree, M.; Rungrotmongkol, T.; Nunthaboot, N.; Aruksakunwong, O.; Intharathep, P.; Decha, P.; Sompornpisut, P.; Hannongbua, S. Source of Oseltamivir Resistance in Avian Influenza H5N1 Virus with the H274Y Mutation. *Amino Acids* **2009**, *37*, 725−732.

(7) Ripoll, D. R.; Khavrutskii, I. V.; Chaudhury, S.; Liu, J.; Kuschner, R. A.; Wallqvist, A.; Reifman, J. Quantitative Predictions of Binding Free Energy Changes in Drug-Resistant Influenza Neuraminidase. *PLoS Comput. Biol.* **2012**, *8*, e1002665.

(8) Sun, H.; Li, Y.; Tian, S.; Wang, J.; Hou, T. P-loop Conformation Governed Crizotinib Resistance in G2032R-Mutated ROS1 Tyrosine Kinase: Clues from Free Energy Landscape. *PLoS Comput. Biol.* **2014**, *10*, e1003729.

(9) Pan, P.; Li, L.; Li, Y.; Li, D.; Hou, T. Insights into Susceptibility of Antiviral Drugs Against the E119G Mutant of 2009 Influenza A (H1N1) Neuraminidase by Molecular Dynamics Simulations and Free Energy Calculations. *Antiviral Res.* **2013**, *100*, 356−364.

(10) Sun, H.; Li, Y.; Li, D.; Hou, T. Insight into Crizotinib Resistance Mechanisms Caused by Three Mutation in ALK Tyrosine Kinase using Free Energy Calculation Approaches. *J. Chem. Inf. Model.* **2013**, *53*, 2376−2389.

(11) Li, L.; Li, Y.; Zhang, L.; Hou, T. Theoretical Studies on the Susceptibility of Oseltamivir against Variants of 2009 A/H1N1 Influenza Neuraminidase. *J. Chem. Inf. Model.* **2012**, *52*, 2715−2729.

(12) Nguyen, H.; Le, L. Steered Molecular Dynamics Approach for Promising Drugs for Influenza A Virus Targeting M2 Channel Proteins. *Eur. Biophys. J.* **2015**, DOI: 10.1007/s00249-015-1047-4.

(13) Sung, J. C.; Wynsberghe, A. W. V.; Amaro, R. E.; Li, W. W.; McCammon, J. A. Role of Secondary Sialic Acid Binding Sites in Influenza N1 Neuraminidase. *J. Am. Chem. Soc.* **2010**, *132*, 2883−2885.

(14) Le, L.; Lee, E. H.; Hardy, D. J.; Truong, T. N.; Schulten, K. Molecular Dynamics Simulations Suggest that Electrostatic Funnel Directs Binding of Tamiflu to Influenza N1 Neuraminidases. *PLoS Comput. Biol.* **2010**, *6*, e1000939.

(15) Fukunishi, Y.; Mikami, Y.; Nakamura, H. The Filling Potential Method: A Method for Estimating the Free Energy Surface for Protein-Ligand Docking. *J. Phys. Chem. B* **2003**, *107*, 13201−13210.

(16) Gervasio, F. L.; Laio, A.; Parrinello, M. Flexible Docking in Solution Using Metadynamics. *J. Am. Chem. Soc.* **2005**, *127*, 2600−2607.

(17) Branduardi, D.; Gervasio, F. L.; Parrinello, M. From A to B in Free Energy Space. *J. Chem. Phys.* **2007**, *126*, 054103.

(18) Fujitani, H.; Tanida, Y.; Matsuura, A. Massively Parallel Computation of Absolute Binding Free Energy with Well-equilibrated State. *Phys. Rev. E* **2009**, *79*, 021914.

(19) Baştuğ, T.; Chen, P. C.; Patra, S. M.; Kuyucak, S. Potential of Mean Force Calculations of Ligand Binding to Ion Channels from Jarzynski's Equality and Umbrella Sampling. *J. Chem. Phys.* **2008**, *128*, 155104.

(20) Fukunishi, Y.; Mitomo, D.; Nakamura, H. Protein - Ligand Binding Free Energy Calculation by the Smooth Reaction Path Generation (SRPG) Method. *J. Chem. Inf. Model.* **2009**, *49*, 1944−1951.
(21) Collins, P. J.; Haire, L. F.; Lin, Y. P.; Liu, J. F.; Russell, R. J.; Walker, P. A.; Skehel, J. J.; Martin, S. R.; Hay, A. J.; Gamblin, S. J. Crystal Structures of Oseltamivir-resistant Influenza Virus Neuraminidase Mutants. *Nature* **2008**, *453*, 1258−1261.
(22) Frisch, M. J.; Trucks, G. W.; Schlegel, H. B.; Scuseria, G. E.; Robb, M. A.; Cheeseman, J. R.; Scalmani, G.; Barone, V.; Mennucci, B.; Petersson, G. A.; Nakatsuji, H.; Caricato, M.; Li, X.; Hratchian, H. P.; Izmaylov, A. F.; Bloino, J.; Zheng, G.; Sonnenberg, J. L.; Hada, M.; Ehara, M.; Toyota, K.; Fukuda, R.; Hasegawa, J.; Ishida, M.; Nakajima, T.; Honda, Y.; Kitao, O.; Nakai, H.; Vreven, T.; Montgomery, J. A., Jr.; Peralta, J. E.; Ogliaro, F.; Bearpark, M.; Heyd, J. J.; Brothers, E.; Kudin, K. N.; Staroverov, V. N.; Kobayashi, R.; Normand, J.; Raghavachari, K.; Rendell, A.; Burant, J. C.; Iyengar, S. S.; Tomasi, J.; Cossi, M.; Rega, N.; Millam, J. M.; Klene, M.; Knox, J. E.; Cross, J. B.; Bakken, V.; Adamo, C.; Jaramillo, J.; Gomperts, R.; Stratmann, R. E.; Yazyev, O.; Austin, A. J.; Cammi, R.; Pomelli, C.; Ochterski, J. W.; Martin, R. L.; Morokuma, K.; Zakrzewski, V. G.; Voth, G. A.; Salvador, P.; Dannenberg, J. J.; Dapprich, S.; Daniels, A. D.; Farkas, Ö.; Foresman, J. B.; Ortiz, J. V.; Cioslowski, J.; Fox, D. J. *Gaussian 09*, Revision D.01; Gaussian, Inc.: Wallingford, CT, 2009.
(23) Morris, G. M.; Huey, R.; Lindstrom, W.; Sanner, M. F.; Belew, R. K.; Goodsell, D. S.; Olson, A. J. Autodock4 and AutoDockTools4: Automated Docking with Selective Receptor Flexibility. *J. Comput. Chem.* **2009**, *30*, 2785−2791.
(24) Humphrey, W.; Dalke, A.; Schulten, K. VMD- Visual Molecular Dynamics. *J. Mol. Graphics* **1996**, *14*, 33−38.
(25) Tian, S.; Sun, H.; Pan, P.; Li, D.; Zhen, X.; Li, Y.; Hou, T. Assessing an Ensemble Docking-Based Virtual Screening Strategy for Kinase Targets by Considering Protein Flexibility. *J. Chem. Inf. Model.* **2014**, *54*, 2664−2679.
(26) Sun, H.; Li, Y.; Shen, M.; Tian, S.; Xu, L.; Pan, P.; Guan, Y.; Hou, T. Assessing the Performance of MM/PBSA and MM/GBSA Methods. 5. Improved Docking Performance using High Solute Dielectric Constant MM/GBSA and MM/PBSA rescoring. *Phys. Chem. Chem. Phys.* **2014**, *16*, 22035−22045.
(27) Tian, S.; Sun, H.; Li, Y.; Pan, P.; Li, D.; Hou, T. Development and Evaluation of an Integrated Virtual Screening Strategy by Combining Molecular Docking and Pharmacophore Searching Based on Multiple Protein Structures. *J. Chem. Inf. Model.* **2013**, *53*, 2743−2756.
(28) Case, D. A.; Pearlman, D. A.; Caldwell, J. W.; Cheatham, T. E.; Wang, J.; Ross, W. S.; Simmerling, C. L.; Darden, T. A.; Merz, K. M.; Stanton, R. V.; Cheng, A. L.; Vincent, J. J.; Crowley, M.; Tsui, V.; Gohlke, H.; Radmer, R. J.; Duan, Y.; Pitera, J.; Massova, I.; Seibel, G. L.; Singh, U. C.; Weiner, P. K.; Kollman, P. A. *AMBER 8*; University of California: San Francisco, CA, 2004.
(29) Wang, J.; Wolf, R. M.; Caldwell, J. W.; Kollman, P. A.; Case, D. A. Development and Testing of a General Amber Force Field. *J. Comput. Chem.* **2004**, *25*, 1157−1174.
(30) Jorgensen, W. L.; Chandrasekhar, J.; Madura, J. D.; Impey, R. W.; Klein, M. L. Comparison of Simple Potential Functions for Simulating Liquid Water. *J. Chem. Phys.* **1983**, *79*, 926−935.
(31) Ryckaert, J. P.; Ciccotti, G.; Berendsen, H. J. C. Numerical Integration of the Cartesian Equations of Motion of a System with Constraints: Molecular Dynamics of n-alkanes. *J. Comput. Phys.* **1977**, *23*, 327−341.
(32) Greengard, L.; Rokhlin, V. A fast algorithm for particle simulations. *J. Comput. Phys.* **1987**, *73*, 325−348.
(33) Wallace, A. C.; Laskowski, R. A.; Thornton, J. M. LIGPLOT: A Program to Generate Schematic Diagrams of Protein-ligand Interactions. *Protein Eng., Des. Sel.* **1995**, *8*, 127−134.
(34) Laskowski, R. A.; Swindells, M. B. LigPlot+: Multiple Ligand - Protein Interaction Diagrams for Drug Discovery. *J. Chem. Inf. Model.* **2011**, *51*, 2778−2786.
(35) The PyMOL Molecular Graphics System, Version 1.7.4; Schrödinger, LLC. https://www.pymol.org (accessed July 2015).
(36) Tran, D.-T. T.; Le, L. T.; Truong, T. N. Discover Binding Pathways Using Sliding Binding-box Docking Approach: Application to Binding Pathways of Oseltamivir to Avian Influenza H5N1 Neuraminidase. *J. Comput.-Aided Mol. Des.* **2013**, *27*, 689−695.
(37) Li, M. S.; Mai, B. K. Steered Molecular Dynamics - a Promising Tool for Drug Design. *Curr. Bioinf.* **2012**, *7*, 342−351.
(38) Nguyen, T. T.; Mai, B. K.; Li, M. S. Study of Tamiflu Sensitivity to Variants of A/H5N1 Virus Using Different Force Fields. *J. Chem. Inf. Model.* **2011**, *51*, 2266−2276.
(39) Srinivasan, J.; Cheatham, T. E., III; Cieplak, P.; Kollman, P. A.; Case, D. A. Continuum Solvent Studies of the Stability of DNA, RNA and Phosphoramidate-DNA Helices. *J. Am. Chem. Soc.* **1998**, *120*, 9401−9409.
(40) Kortemme, T.; Baker, D. A Simple Physical Model for Binding Energy Hot Spots in Protein-protein Complexes. *Proc. Natl. Acad. Sci. U. S. A.* **2002**, *99*, 14116−14121.
(41) Moscona, A. Oseltamivir Resistance-Disabling Our Influenza Defenses. *N. Engl. J. Med.* **2005**, *353*, 2633−2636.

DOI: 10.1021/acs.jcim.5b00319
J. Chem. Inf. Model. 2015, 55, 1936−1943